Acta Crystallographica Section D
Biological Crystallography
ISSN 0907-4449

Two-photon excited UV fluorescence for protein crystal detection

Jeremy T. Madden, Emma L. DeWalt and Garth J. Simpson*

Department of Chemistry, Purdue University, 560 Oval Drive, West Lafayette, IN 47907, USA

Correspondence e-mail: gsimpson@purdue.edu

Received 14 April 2011
Accepted 14 July 2011

Two-photon excited ultraviolet fluorescence (TPE-UVF) microscopy is explored for sensitive protein-crystal detection as a complement to second-order nonlinear optical imaging of chiral crystals (SONICC). Like conventional ultraviolet fluorescence (UVF), TPE-UVF generates image contrast based on the intrinsic fluorescence of aromatic residues, generally producing higher fluorescence emission within crystals than the mother liquor by nature of the higher local protein concentration. However, TPE-UVF has several advantages over conventional UVF, including (i) insensitivity to optical scattering, allowing imaging in turbid matrices, (ii) direct compatibility with conventional optical plates and windows by using visible light for excitation, (iii) elimination of potentially damaging out-of-plane UV excitation, (iv) improved signal to noise through background reduction from out-of-plane excitation and (v) relatively simple integration into instrumentation developed for SONICC.

1. Introduction

Identification of conditions for generating diffraction-quality protein crystals is the major cost in terms of time and expense for protein structure determination by X-ray crystallography. Reduction in the detection limits for protein crystallization screenings can reduce both the quantity of protein used and the time required for the initial screenings. Before high-resolution X-ray diffraction images can be generated, hundreds of crystallization conditions are typically screened and imaged to identify and optimize conditions for crystal growth. Conventional screening techniques include bright-field imaging (Echalier *et al.*, 2004), trace fluorescence labeling or passive doping (Groves *et al.*, 2007; Forsythe *et al.*, 2006) and one-photon excited UV fluorescence (UVF; Judge *et al.*, 2005; Dierks *et al.*, 2010). For automated scoring, bright-field techniques generally rely on image-analysis algorithms to detect protein crystals (Andrey *et al.*, 2004). However, reliable scoring of bright-field images can be challenging because of the poor selectivity for crystals and the relatively low intrinsic information content in the images (Bern *et al.*, 2004). The situation is improved significantly by coupling bright-field imaging with fluorescence. However, trace labeling requires protein modification by incorporation of a fluorophore (Forsythe *et al.*, 2006). UVF offers significant advantages over trace labeling as it exploits the intrinsic fluorescence that is present in almost all proteins from the aromatic amino acids (*e.g.* exciting the tryptophan residues at around 280 nm and detecting the emission at 320–350 nm). Furthermore, intrinsic UVF provides a means to discriminate nonfluorescent salt crystals and small-molecule crystals from protein crystals with

relative ease and without the need for fluorescence labeling. Despite these advantages, UV fluorescence is not without its own practical limitations. UV fluorescence produces signals arising from both protein crystals and amorphous protein aggregates that may have formed (Vernede *et al.*, 2006; Wampler *et al.*, 2008). Furthermore, cover slips and films used to seal the crystallization plates decrease or block the incident UV light, contributing to signal attenuation (Gill, 2010). Large backgrounds from out-of-plane fluorescence from the cover slip and/or solvated protein can further frustrate reliable detection of protein crystals and degrade the signal-to-noise ratio (S/N) for crystal detection. Finally, UV photodamage of the proteins can arise during prolonged (several seconds) excitation with UV radiation (Chen *et al.*, 2009; Vernede *et al.*, 2006), which can be problematic for the detection of small protein crystals, for proteins exhibiting weak UV-excited fluorescence and for samples imaged repeatedly over time. Tryptophan absorbance has also been explored to provide contrast for detection of protein crystals to overcome interference from fluorescence quenching (Gill, 2010). However, both absorption and scatter can result in a reduction of transmitted light and the two competing effects can be potentially challenging to separate.

Second-order nonlinear imaging of chiral crystals, or SONICC, which utilizes the nonlinear optical process of second-harmonic generation (SHG) to detect protein crystals, has recently been developed (Kissick *et al.*, 2010, 2011). With the exception of the relatively rare cubic gyroidal symmetry class, SHG signals are symmetry allowed in protein crystals but forbidden in solutions and amorphous aggregates lacking long-range order (Shen, 2003; Boyd, 2008; Kissick *et al.*, 2010, 2011), which permits highly selective detection of crystals. SONICC also shares one of the advantages of multi-photon fluorescence microscopy by enabling reliable imaging in turbid matrices, such as lipidic cubic phase (LCP), without loss of image quality (Kissick *et al.*, 2010). However, SONICC signals generally increase with lower crystal symmetry, potentially producing relatively weak signals for crystals with high-symmetry space groups. In addition, the presence of non-centrosymmetric crystals of salts or precipitants that may grow from the mother liquor can also produce SHG responses, potentially interfering in the detection of protein crystals.

The confidence in any measurement is improved significantly if the same outcome is observed using multiple independent methods to reduce complications from bias and artifacts. Two-photon excited UV fluorescence (TPE-UVF) has the potential to serve as a useful complement to SONICC characterization, while circumventing many of the complications arising in conventional UVF. Two-photon excitation only results in excitation and emission within the focal volume, essentially eliminating the background from out-of-plane fluorescence arising in conventional UV detection. TPE-UVF allows excitation with visible light and detection in the near-UV to visible range, such that UV transparency is not required in either the crystallization plate or the microscope objective. Combining SONICC with TPE-UVF on the same instrument platform can permit complementary measurements, giving crystallinity and chemical information, respectively. This combination can reduce the uncertainty associated with protein-crystal detection. UV photodamage is expected to be

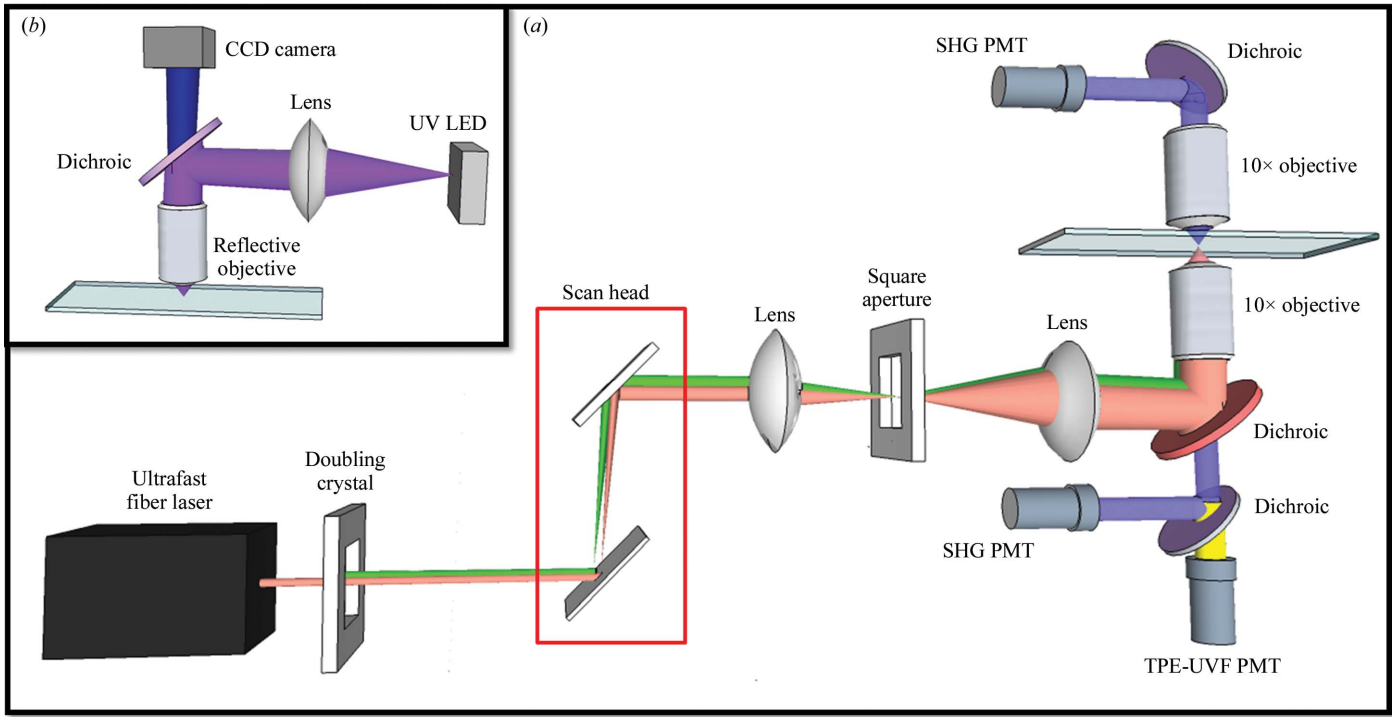

Figure 1
Instrument schematics for (*a*) SONICC and TPE-UVF measurements, with insertion of doubling crystal allowing two-photon excitation, and (*b*) conventional one-photon (UV) measurements.

substantially reduced in TPE-UVF by the virtual elimination of out-of-plane excitation. Finally, TPE-UVF should enable the detection of protein crystals in turbid media, as only the unscattered 'ballistic' light reaching the focal plane contributes to the measured fluorescence. The present study is designed to demonstrate TPE-UVF imaging of protein crystals and to assess the merits of combined TPE-UVF and SONICC analysis for protein-crystal detection.

2. Experimental

Serving as a complementary technique to SONICC, the instrument utilized for these studies can be adapted for both SONICC and TPE-UVF measurements without the need for UV optics and with little modification needed to switch between techniques. Instrumentation schematics for TPE-UVF and SONICC can be seen in Fig. 1(*a*) and for UV fluorescence measurements in Fig. 1(*b*).

2.1. Excitation sources

For both TPE-UVF and SONICC studies, the fundamental beam was generated by a mode-locked free-space coupled Uranus fiber laser (Polaronyx) at 1030 nm, ~200 fs pulses, 76 MHz and 3–350 mW average power during imaging. A second-harmonic generation (SHG) unit placed after the free-space coupler allowed the fundamental light to be directed through a doubling crystal to generate 515 nm at ~300 fs. Based on previous multi-photon fluorescence studies of the aromatic amino acids (Rehms & Callis, 1993), tryptophan dominates the two-photon excitation spectrum and produces a local maximum at 560 nm (corresponding to a two-photon energy equivalent of 280 nm light). However, significant TPE-UVF can still arise from tyrosine and phenylalanine. From the published TPE spectra, TPE-UVF of tryptophan with 515 nm light is expected to be ~20% lower than the local maximum expected at 560 nm (Rehms & Callis, 1993), with a TPE-UVF cross-section of ~32 mGM (1 GM = 10^{-50} cm^4 s^{-1} photon^{-1} per molecule) at 532 nm (Sengupta *et al.*, 2001). In one set of SONICC experiments, a Spectra-Physic Mai-Tai tunable ultrafast laser provided 800 nm, 125 fs pulses, 80 MHz and 25–125 mW average power during imaging. For conventional UVF imaging, a nine-LED array collimated using a spherical lens provided 5 mW of incident power at 280 nm. The incident light entered an upright Zeiss microscope (Axioskop 50) base through the top port, was reflected by a 266 nm DC mirror (Chroma) and was focused onto the sample using a reflective objective (Newport, 15×, 0.4 NA, infinity corrected). The resulting visible fluorescent signal was collected in the epi direction and was captured using a high-resolution USB CCD camera (Thorlabs).

2.2. TPE-UVF/SONICC instrumentation

SONICC images were acquired using a custom-designed beam path, with a resonant vibrating mirror (~7.8 kHz) and a galvanometer performing beam scanning along the fast and slow axes, respectively. The resulting beam was directed to a Nikon microscope base (TE2000) in the inverted configuration by multiple silvered and dichroic mirrors (Chroma) and telecentric lens pairs. The beam was then focused onto the sample using a 10× objective (Nikon Plan Fluor, 0.3 NA). Underfilling of the objective produced a depth of field of ~80 µm. For SONICC measurements, the fundamental beam was directed to the objective by a dichroic mirror with a reflectance band between 900 and 1300 nm and the resulting second-harmonic (SH) signal was detected by photomultiplier tubes (PMT, Burle) in the epi and transmission direction using dichroic mirrors (Chroma) centered around 515 nm and through a set of filters composing of a KG3 (Thorlabs), 500 nm longpass (LP; Edmund Optics) and 515 nm bandpass (BP; Chroma). The coherent nature of SHG generally results in greater signal intensities in the transmitted direction. Complementary detection in the epi direction can provide additional information on size and allows imaging in platforms for which collection in transmission is impractical. With two conventional 10× objectives as used in this work, the distance between the objectives was ~50 mm, limiting the crystallization platforms to be used to less than that number. However, long working-distance objectives with ~50 mm working distances and comparable numerical aperture are also widely available.

For TPE-UVF measurements, the incident beam, now doubled to 515 nm, was directed towards the objective by a dichroic with a reflectance band from 450 to 550 nm and the resulting TPE-UVF signal was detected in the epi direction with a PMT (Hamamatsu, R1924A) through a filter set consisting of a 515 nm notch (Semrock), 360 nm BP (Chroma) and UV-absorbing black filter (Edmund Optics). This selection of optics and filters was chosen to allow efficient excitation of the aromatic amino-acid residues through the two-photon equivalent wavelength of 257.5 nm and selective detection of the broadband red-shifted fluorescence emission from ~340 to 380 nm. The fundamental beam was directed to a galvanometer scanner (Cambridge Technology) by kinematically controlled silver mirrors. Epi bright-field images were captured using a visible LED and a color CMOS camera (Thorlabs). Image collection was completed using custom-made *Labview* software, allowing the number of sweeps of the resonant mirror and the galvanometer range to be selected. The final image sizes and acquisition times varied, but were approximately 150 pixels on the fast scan axis and 200 pixels on the slow axis, corresponding to a field of view of 620 × 450 µm. Acquisition times for full frames ranged from 3 to 120 s (depending upon the number of sweeps of the resonant mirror). *ImageJ* was used for analysis and resizing of the images for overlay.

3. Sample materials and methods

Select samples were explored for both proof-of-concept measurements and to address the caveats and advantages offered by TPE-UVF and SONICC. Sodium citrate, potassium sodium tartrate, tryptophan and egg-white lysozyme were purchased directly from Sigma–Aldrich. Catalase crystals

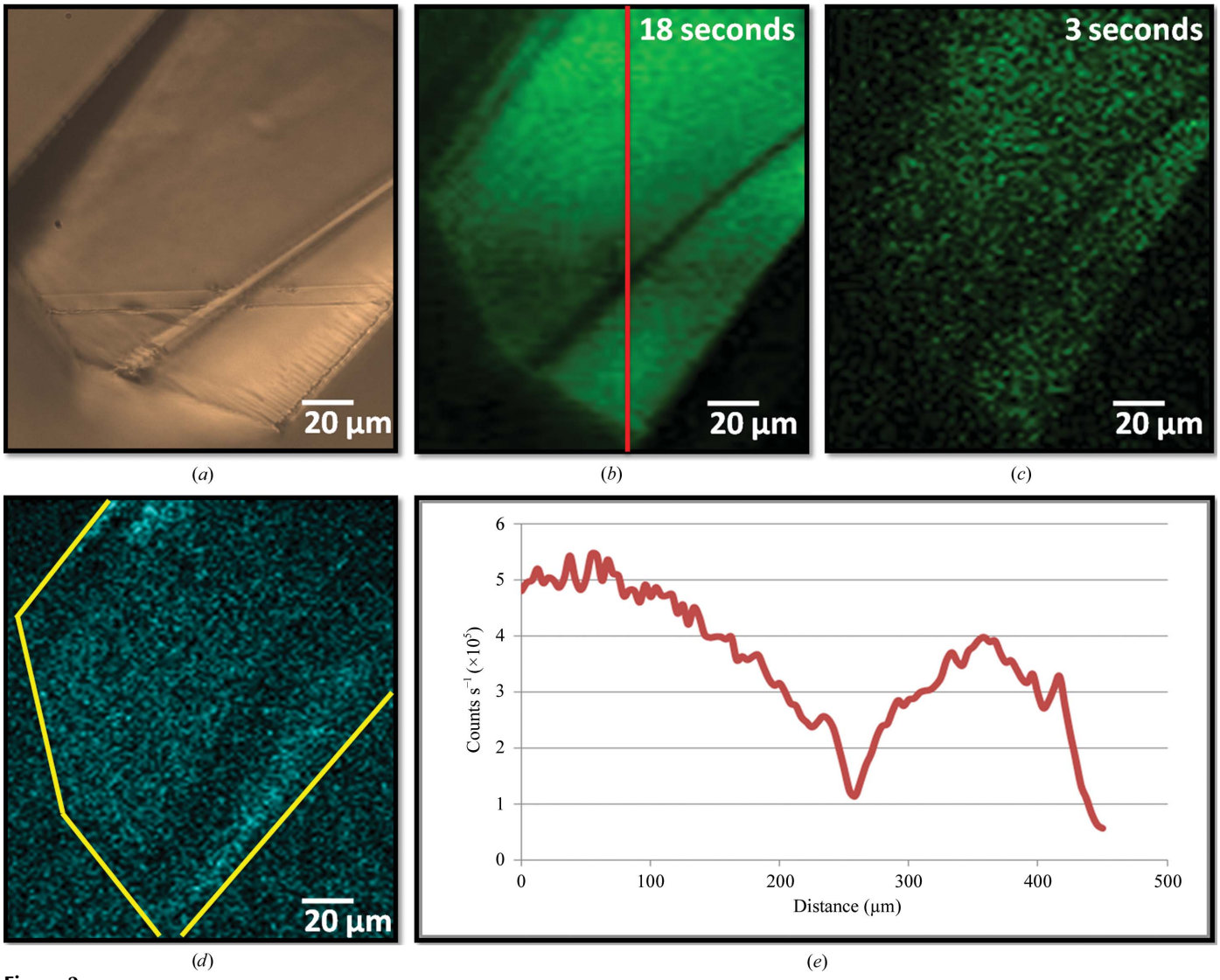

Figure 2
Comparison of different imaging methods for a lysozyme crystal: (*a*) bright-field and corresponding TPE-UVF measurements at 25 mW incident power and (*b*) 18 s and (*c*) 3 s acquisition. (*d*) Complementary SONICC measurements gave a weak signal, peaking at 10 000 counts s^{-1} for ∼230 mW incident power. (*e*) Analysis of the TPE-UVF measurements, as indicated by the red line, shows a bright signal, producing >500 000 counts s^{-1} for 25 mW incident power.

were grown in a pH 5.3, 50 m*M*, 10 ml buffer solution ($\mu = 0.2$) of KH_2PO_4/Na_2HPO_4 (0.35 ml:0.036 ml) made to volume with ultrapure deionized water (Barnstead) and allowed to crystallize over several days. Crystals of *Escherichia coli* maltose transporter, an ATP-binding cassette (ABC) transporter, were grown by mixing the protein sample with a reservoir solution consisting of 29% polyethylene glycol 400, 50 m*M* NaCl, 40 m*M* $MgCl_2$, 100 m*M* Na HEPES buffered to pH 7.5 at a 1:1 ratio in sitting drops by vapor diffusion at 293 K. Bright-field and TPE-UVF images were obtained directly on protein samples in the 96-well plates in which the crystals were grown. Bright-field, TPE-UVF and SONICC measurements were also obtained on protein and salt samples transferred to glass slides, as certain crystals were not crystallized in well plates. UVF measurements required remounting hanging drops between two glass slides and an O-ring, as the well plates attenuated the incident light.

4. Results

Initial TPE-UVF studies were performed for pure L-tryptophan powder (see Supplementary Material[1]). Bright TPE-UVF signals were observed for the pure powder. The TPE-UVF signal as a function of incident intensity measured at two different regions within the field of view produced a slope of 2.0 ± 0.1 in a log–log plot, indicating a quadratic dependence between the detected fluorescence and the incident power, consistent with two-photon excitation.

TPE-UVF and SONICC measurements of lysozyme crystals are shown in Fig. 2. Lysozyme contains six tryptophan residues per protein copy, which are likely to dominate the detected fluorescence emission (Beechem & Brand, 1985). Large

[1] Supplementary material has been deposited in the IUCr electronic archive (Reference: MH5044). Services for accessing this material are described at the back of the journal.

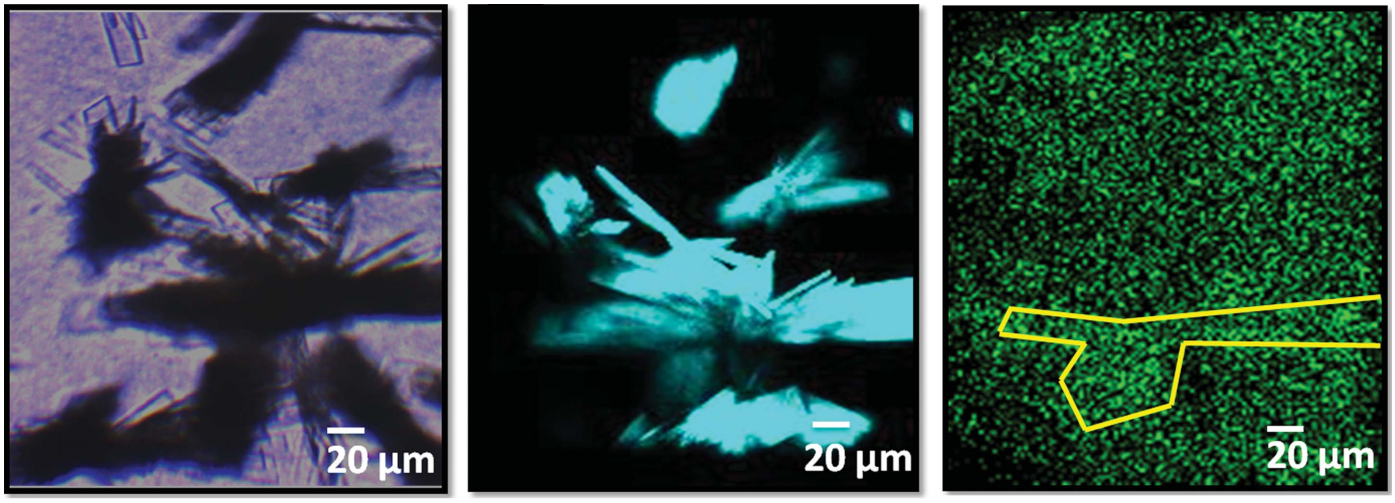

(*a*) (*b*) (*c*)

Figure 3
Inpact of fluorescence quenching: (*a*) bright-field, (*b*) SONICC and (*c*) TPE-UVF measurements of catalase crystals, with bright SHG images being generated at low power but minimal TPE-UVF signal being generated even at incident powers of >40 mW and an acquisition time of 2 min. This trend is attributed to quenching of the TPE-UVF signal by the heme chromophore in catalase.

fluorescence signals from the protein crystals were observed at low power (Fig. 2*b*), with detectable signal evident with just 3 s acquisition time (Fig. 2*c*). Complementary SONICC measurements of similarly prepared lysozyme crystals are also shown in Fig. 2(*d*). Consistent with previously noted expectations, the relatively high $P4_32_12_1$ symmetry of the lysozyme lattice and a propensity to orient with the crystallographic *z* axis normal to the substrate surface and parallel to the direction of beam propagation combine to produce relatively weak SONICC signals under the most common experimental configurations.

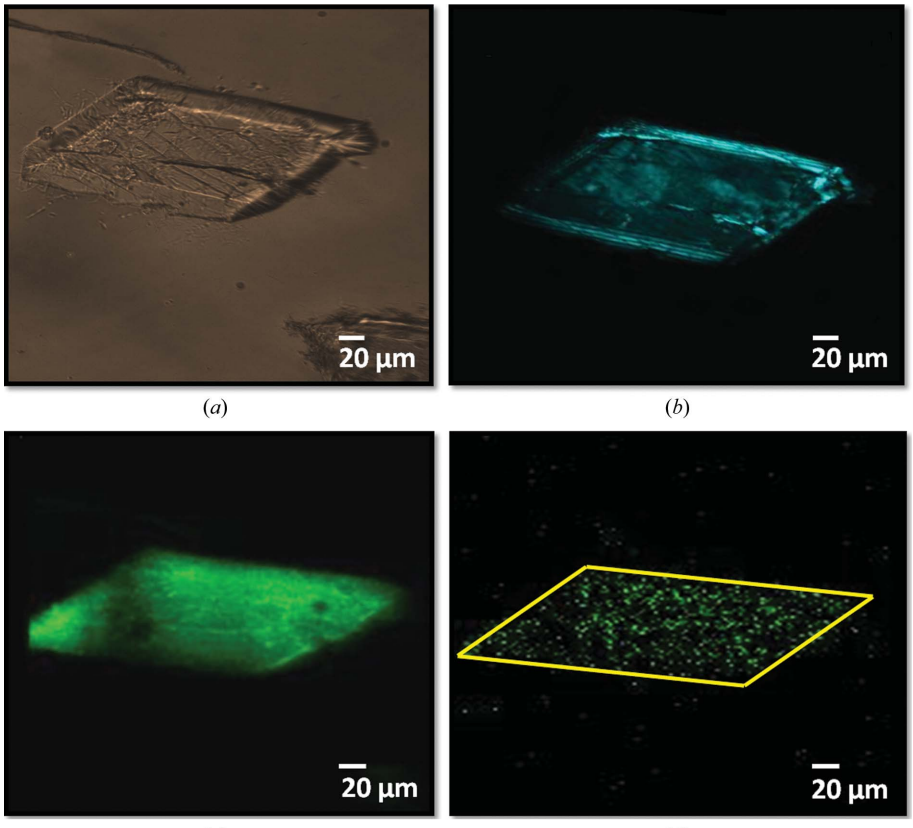

(*a*) (*b*) (*c*) (*d*)

Figure 4
Crystal detection of an ABC maltose transporter protein: (*a*) bright field, (*b*) SONICC and TPE-UVF at both (*c*) 3 min and (*d*) 3 s acquisition time. Complementary SONICC and TPE-UVF measurements demonstrate that the sample is likely to be both crystalline and comprised of protein.

It is reasonably well established that the presence of a quenching agent within a protein can dramatically impact both the lifetime and the quantum yield for UV fluorescence (Kehoe *et al.*, 2008). Measurements to test the impact of quenching agents on TPE-UVF were performed using crystals of catalase, which contains a nonfluorescent iron heme group exhibiting strong absorption that overlaps with the intrinsic fluorescence emission profile of tryptophan (∼350–380 nm). TPE-UVF and SONICC images of catalase crystals are shown in Fig. 3. Consistent with expectations, the TPE-UVF measurements produced only weak signals for catalase. In contrast, the SONICC measurements were quite bright, approaching saturation of photon-counting statistics even with 100 mW incident power.

In principle, TPE-UVF is expected to allow imaging through UV-opaque windows and materials, since the incident light is in the visible and the detected light is Stokes-shifted to the near-UV. This capability was explored by direct comparisons of UVF, TPE-UVF and SONICC on crystals of an ABC maltose transporter imaged in

both sealed glass slides and a crystallization plate (96-well plate with two-drop chamber format, chamber drop volume of 10 nl to 5 µl and main drop volume of 50–100 µl). Fig. 4(*a*) shows a bright-field image of an ABC maltose transporter crystal mounted on a sealed glass slide. Consistent with the presence of crystallinity, SONICC measurements produced relatively strong signals and high contrast images, as seen in Fig. 4(*b*). The presence of fringes observed at the edges of the crystal is consistent with the positive and negative interference of the coherent SHG signal. Corresponding TPE-UVF measurements in Fig. 4(*c*) produced a signal-to-background ratio (S/B) of over 450 for >100 mW incident power and 2–3 min acquisition time. Signal from these crystals is evident over the background even with an acquisition time of only 3 s at 50 mW incident power (Fig. 4*d*). Single-crystal XRD measurements performed at a synchrotron source confirmed that crystals prepared under similar conditions were comprised of protein and diffracted to a resolution of ∼2 Å (Orelle *et al.*, 2010).

TPE-UVF measurements were conducted on ABC maltose transporter crystals grown in a 96-well crystallization plate (Fig. 5*b*). Imaged through the crystallization-well cover slip, these *in situ* measurements produced an S/B of 28 at moderate laser fluences (Fig. 5*c*). In comparison, conventional UVF measurements produced no detectable fluorescence from the crystals when imaged *in situ* within the sealed wells, even for integration times of 250 ms at 2.50 frames s^{-1}. This can presumably be attributed to UV attenuation and background fluorescence arising from absorption by the cover slip. UVF images were only obtained after breaking the seal of the cover slip and extracting a crystal from those previously imaged by TPE-UVF (Fig. 5*e*). The resulting sample, mounted on a sealed glass slide in the mother liquor, generated an S/B of 10, significantly less than that from the TPE-UVF measurements (Fig. 5*f*).

5. Discussion

Confidence in a measurement increases significantly when similar outcomes are achieved using orthogonal measurement approaches. With multiple methods, the combined measurements become less sensitive to false positives and negatives that can potentially arise from systematic errors in any one approach. The measurements and samples investigated in this study were purposely designed to challenge reliable crystal detection by TPE-UVF and SONICC in order to characterize the conditions that are likely to result in the observation of false negatives and false positives for protein-crystal

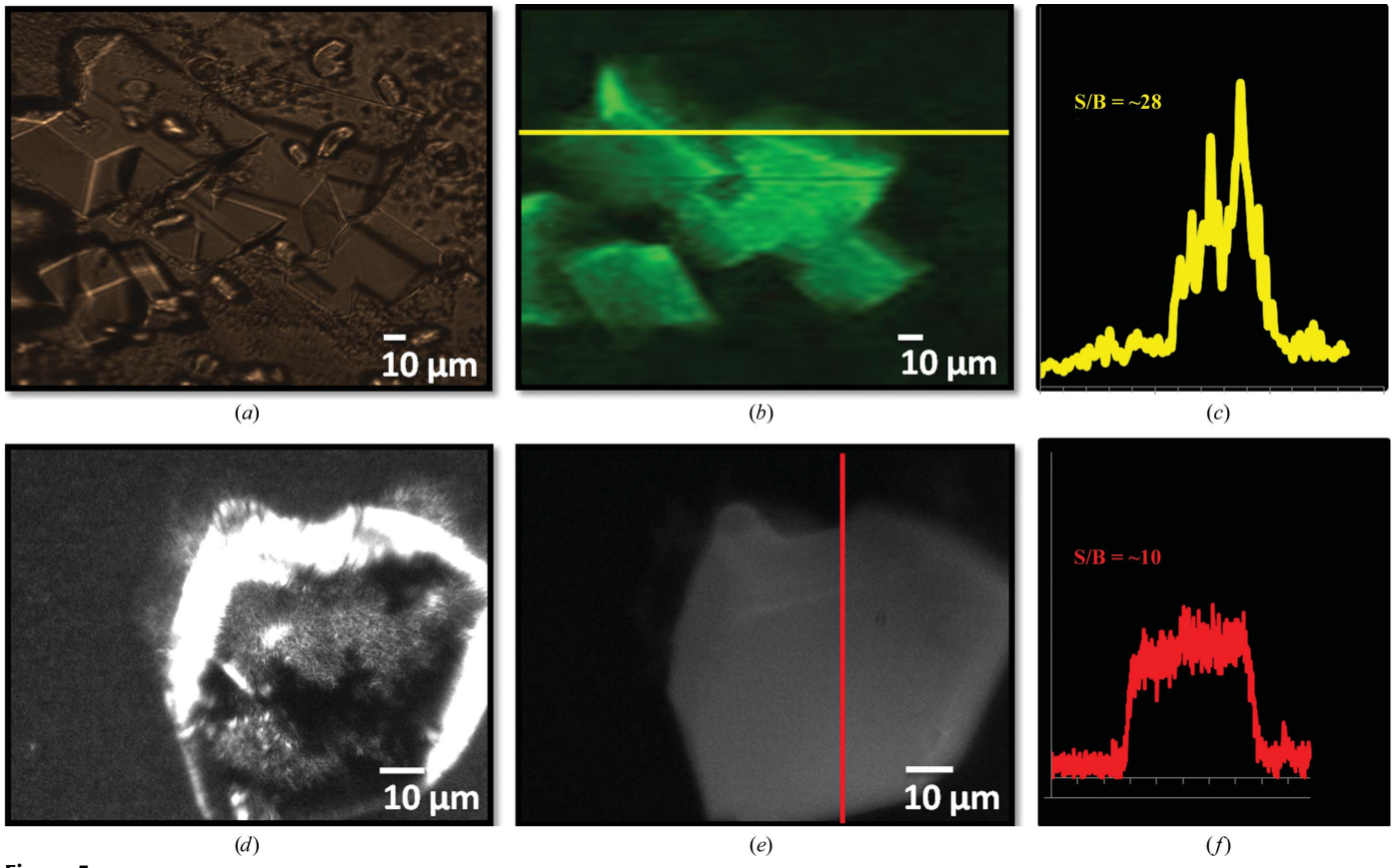

Figure 5
Comparison of one- and two-photon excited UVF of an ABC maltose transporter membrane-protein crystal: (*a*) bright-field and (*b*) TPE-UVF measurements completed *in situ* through the crystallization-plate cover slip; (*c*) shows a corresponding line scan analysis showing high signal to background for moderate laser power. (*d*) Bright-field and (*e*) conventional UVF measurements on the same crystals performed after breaking the well seal and extracting a crystal to allow UVF. (*f*) Corresponding line scan analysis indicates weaker signal to background compared with TPE-UVF measurements.

detection. For example, lysozyme presents an interesting case when performing complementary measurements using TPE-UVF and SONICC. Owing to the high $P4_32_12_1$ symmetry of lysozyme crystals anticipated under the experimental conditions and their tendency to grow along the axis of light propagation, SONICC measurements resulted in poor contrast between crystalline lysozyme and the mother liquor with 225 mW incident power (Fig. 2*d*). Similarly, TPE-UVF generated only relatively weak signals from catalase owing to internal fluorescence quenching. In addition, not all proteins contain aromatic residues, in which case both UVF and TPE-UVF signals may be relatively weak or absent. However, complementary measurements by SONICC still allowed reliable crystal detection with high S/B. From these measurements, the complementary combination of TPE-UVF and SONICC may offer substantial improvements in automated scoring in protein crystallization trials, with high confidence in minimizing both false negatives and false positives.

Although not explicitly confirmed in this work, it is anticipated that TPE-UVF should be expected to substantially reduce UV-induced photodamage to proteins during imaging. UV damage has been implicated in the damage of proteins, specifically by the mechanisms of photolysis and photo-oxidation (Gill, 2010; Vernede *et al.*, 2006; Kehoe *et al.*, 2008). In conventional UVF the full field of view is illuminated simultaneously, together with all the proteins present above and below the focal plane. In contrast, beam-scanning TPE-UVF excites fluorescence only within a volume consisting of a few femtolitres at any one time and is limited exclusively to excitation within the focal plane. By restricting excitation to just the volumes over which images are to be generated, TPE-UVF effectively eliminates undesirable excitation of proteins out of the focal plane or outside the field of view of the image. Furthermore, the reduction in background associated with the intrinsically confocal nature of TPE-UVF combined with single-photon-counting detection methods allows high-contrast images to be generated with much lower fluorescence photon fluxes than are typically required for conventional UVF. Following excitation, each aromatic amino acid has a finite probability of generating fluorescence or undergoing damaging reactions. Images constructed from fewer fluorescent photons within the field of view and negligible out-of-plane excitation should correspond to a lower anticipated UV-induced defect density. Beam-scanning raises the possibility of alternative damage mechanisms not present in conventional UVF from local heating (*e.g.* arising from nonradiative relaxation). By using a resonant scanner, the illumination time per confocal volume per pass was short (50 ns or $\sim$4 laser pulses) to minimize local heating effects, with retraces of the beam over the same area performed to increase the S/N. However, detailed studies of laser-induced damage are certainly warranted to more rigorously quantify such effects.

The substantial improvements in image contrast when comparing one-photon and two-photon excitation images in Fig. 5 provides experimental evidence supporting the minimization of out-of-plane fluorescence consistent with these expectations. Here, the background suppression and the improvement in image contrast also has direct benefits for applications targeting automated crystal detection and analysis in high-throughput platforms. Reliable scoring of crystallization trials based on conventional imaging methods remains largely elusive. Difficulties hinge largely around the presence of relatively frequent false-positive and false-negative hits when relying on analysis of low-contrast methods such as those obtained by bright-field imaging and/or UVF. The measured improvement in image contrast by TPE-UVF has the potential to significantly improve the reliability of scoring algorithms in automated applications.

As demonstrated in this work, remarkably few modifications needed to be performed to alternate between SONICC and TPE-UVF measurements using a single microscope and detection electronics package. In these studies, both of these measurements were completed using the same software, detectors and laser, with filters and mirrors being used to alter the incident and detected wavelengths. All other optics and objectives for each set of measurements were identical. Notably, conventional objectives corrected for the visible can be used for both TPE-UVF and SONICC measurements. By simple optical automation, such as sample scanning using a computerized *xy* stage and *z*-scanning using motorized focus control (Levene *et al.*, 2004; Gualtieri *et al.*, 2011), this capability could potentially facilitate fast analysis and screenings of crystallization plates with minimal time between measurements and without requiring sample transfer.

These two techniques can discriminate between salt and protein crystals, as salt crystals do not contain aromatic residues and a large percentage have space groups that are not SHG active (see Supplementary Material). Although certain salts, such as chiral tartrates, are SHG active, the complementary detection schemes permit the selective detection of protein crystals, as non-aromatic salts will not be excited using TPE-UVF, and aggregates and solutions will not be excited using SONICC.

TPE-UVF accesses comparable information as conventional UV fluorescence, but overcomes many of the practical limitations associated with the technique, including (i) direct compatibility with conventional windows and cover slips, (ii) reduction of background from out-of-plane fluorescence and (iii) minimization of photodamage by suppression of out-of-plane excitation. As excitation occurs with visible light, UV attenuation by conventional cover slips and crystallization films is not relevant. This multiphoton process also minimizes background signal by virtually eliminating out-of-plane fluorescence, providing high-contrast visualization of protein crystals while reducing UV-induced photodamage.

TPE-UVF can be expected to share the same insensitivity to optical scatter as both SONICC and visible TPEF measurements. Like all processes scaling quadratically or higher with incident intensity, only the unscattered light surviving the path to the focal volume can significantly contribute to the detected signal (Balu *et al.*, 2009; Beaurepaire *et al.*, 2001; Helmchen & Denk, 2005; Leray & Mertz, 2006; Oheim *et al.*, 2001; Svoboda & Yasuda, 2006; Denk *et al.*,

1990). Once the signal is generated in the focal volume, scattering can result in an attenuation of the signal but does not contribute to background or impact spatial resolution in the resulting image, as the focal volume is the only likely origin for the signal.

Sample-acquisition times for both SONICC and TPE-UVF measurements ranged from 3 to 120 s per frame. However, these acquisition times were dictated by the requirement of a relatively large (∼500 µm) field of view and, for a majority of the experiments, limited (<40 mW) excitation power. Video-rate acquisitions of multi-photon excited fluorescence and nonlinear optical images are now commonplace using a variety of methods (Fan *et al.*, 1999; Zipfel *et al.*, 2003; Roorda *et al.*, 2004). Similar acquisition times for TPE-UVF measurements can be reasonably expected if conducted with higher incident power using dedicated acquisition electronics and automated sample repositioning.

6. Conclusion

In summary, visualization of protein crystals has been accomplished through multi-photon excitation of the inherent aromatic residues using TPE-UVF and through SONICC. The use of TPE-UVF for protein-crystal detection, specifically for complementary detection with SONICC and bright-field imaging, provided increased sensitivity and signal to background. Having compatibility with conventional optics, the advantages that two-photon fluorescence detection of protein crystals offers can provide fast and efficient screening of crystallization trays and samples, decreasing the time associated with one of the major bottlenecks of X-ray crystallography.

The authors acknowledge Michael Oldham and Guimei Yu for providing protein samples. Graduate-student funding and instrumentation development was supported in part by the Center for Direct Catalytic Conversion of Biomass to Biofuels (C3Bio), an Energy Frontier Research Center funded by the US Department of Energy, Office of Science, Office of Basic Energy Sciences, Award No. DE-SC0000997, and instrumentation development was supported in part by the NIH Research Project Grant Program (RO1) 1RO1RR026273-01.

References

Andrey, P., Lavault, B., Cipriani, F. & Maurin, Y. (2004). *J. Appl. Cryst.* **37**, 265–269.
Balu, M., Baldacchini, T., Carter, J., Krasieva, T. B., Zadoyan, R. & Tromberg, B. J. (2009). *J. Biomed. Opt.* **14**, 010508.
Beaurepaire, E., Oheim, M. & Mertz, J. (2001). *Opt. Commun.* **188**, 25–29.
Beechem, J. M. & Brand, L. (1985). *Annu. Rev. Biochem.* **54**, 43–71.
Bern, M., Goldberg, D., Stevens, R. C. & Kuhn, P. (2004). *J. Appl. Cryst.* **37**, 279–287.
Boyd, R. W. (2008). *Nonlinear Optics*, 3rd ed. New York: Elsevier.
Chen, J., Callis, P. R. & King, J. (2009). *Biochemistry*, **48**, 3708–3716.
Denk, W., Strickler, J. H. & Webb, W. W. (1990). *Science*, **248**, 73–76.
Dierks, K., Meyer, A., Oberthür, D., Rapp, G., Einspahr, H. & Betzel, C. (2010). *Acta Cryst.* F**66**, 478–484.
Echalier, A., Glazer, R. L., Fülöp, V. & Geday, M. A. (2004). *Acta Cryst.* D**60**, 696–702.
Fan, G. Y., Fujisaki, H., Miyawaki, A., Tsay, R.-K., Tsien, R. Y. & Ellisman, M. H. (1999). *Biophys. J.* **76**, 2412–2420.
Forsythe, E., Achari, A. & Pusey, M. L. (2006). *Acta Cryst.* D**62**, 339–346.
Gill, H. S. (2010). *Acta Cryst.* F**66**, 364–372.
Groves, M. R., Müller, I. B., Kreplin, X. & Müller-Dieckmann, J. (2007). *Acta Cryst.* D**63**, 526–535.
Gualtieri, E. J., Guo, F., Kissick, D. J., Jose, J., Kuhn, R. J., Jiang, W. & Simpson, G. J. (2011). *Biophys. J.* **100**, 207–214.
Helmchen, F. & Denk, W. (2005). *Nature Methods*, **2**, 932–940.
Judge, R. A., Swift, K. & González, C. (2005). *Acta Cryst.* D**61**, 60–66.
Kehoe, J. J., Remondetto, G. E., Subirade, M., Morris, E. R. & Brodkorb, A. (2008). *J. Agric. Food Chem.* **56**, 4720–4725.
Kissick, D. J., Gualtieri, E. J., Simpson, G. J. & Cherezov, V. (2010). *Anal. Chem.* **82**, 491–497.
Kissick, D. J., Wanapun, D. & Simpson, G. J. (2011). *Annu. Rev. Anal. Chem.* **4**, 419–437.
Leray, A. & Mertz, J. (2006). *Opt. Express*, **14**, 10565–10573.
Levene, M. J., Dombeck, D. A., Kasischke, K. A., Molloy, R. P. & Webb, W. W. (2004). *J. Neurophysiol.* **91**, 1908–1912.
Oheim, M., Beaurepaire, E., Chaigneau, E., Mertz, J. & Charpak, S. (2001). *J. Neurosci. Methods*, **111**, 29–37.
Orelle, C., Alvarez, F. J., Oldham, M. L., Orelle, A., Wiley, T. E., Chen, J. & Davidson, A. L. (2010). *Proc. Natl Acad. Sci. USA*, **107**, 20293–20298.
Rehms, A. A. & Callis, P. R. (1993). *Chem. Phys. Lett.* **208**, 276–282.
Roorda, R. D., Hohl, T. M., Toledo-Crow, R. & Miesenböck, G. (2004). *J. Neurophysiol.* **92**, 609–621.
Sengupta, P., Balaji, J., Mukherjee, S., Philip, R., Kumar, G. R. & Maiti, S. (2001). *Proc. SPIE*, **4262**, 336–339.
Shen, Y. R. (2003). *The Principles of Nonlinear Optics.* New Jersey: John Wiley & Sons.
Svoboda, K. & Yasuda, R. (2006). *Neuron*, **50**, 823–839.
Vernede, X., Lavault, B., Ohana, J., Nurizzo, D., Joly, J., Jacquamet, L., Felisaz, F., Cipriani, F. & Bourgeois, D. (2006). *Acta Cryst.* D**62**, 253–261.
Wampler, R. D., Kissick, D. J., Dehen, C. J., Gualtieri, E. J., Grey, J. L., Wang, H.-F., Thompson, D. H., Cheng, J.-X. & Simpson, G. J. (2008). *J. Am. Chem. Soc.* **130**, 14076–14077.
Zipfel, W. R., Williams, R. M. & Webb, W. W. (2003). *Nature Biotechnol.* **21**, 1369–1377.